F. Méot

FFAG 2019 Workshop - FFAG School
A Tutorial on the Raytracing Code Zgoubi

Theory, reminder: pp. 2-10, including in particular spiral sector pp. 9-10.

The exercises we'll do (after RAL studies): pp. 14-15.
Solutions pp. 17-23.

PSI, Nov. 19-22, 2019

List of Abbreviations

List of Abbreviations

A	sector angle of a magnet
B_o	field value at the reference radius R_0
B_y	axial component of the magnetic field
$B\rho = p/q;\ B\rho_0$	particle rigidity; reference rigidity at R_0
E; E_s	particle energy; synchronous
$F = \frac{\overline{B^2}}{\overline{B}^2}$	flutter
$\mathcal{F}(\theta)$	azimuthal field form factor, or "flutter" factor
h	RF harmonic number
$k = \frac{r}{B}\frac{dB}{dr} \approx -n\frac{r}{\rho}$	scaling index
$\mathcal{L}$	magnetic length
m_0	particle rest mass
N	number of cells in a ring, or ring periodicity
$n = -\frac{\rho}{B}\frac{dB}{dx}$	field index
pf	packing factor, *i.e.*. bend length over orbit length
$p;\ p_0$	particle momentum; reference momentum
q	particle charge
$R;\ R_0$	average orbit radius = $\mathcal{S}/2\pi$; (arbitrary) reference value
$r,\ \theta$	radial and azimuthal coordinates$^{(a)}$
$\mathcal{S}, \mathcal{S}_0$	closed orbit length=$2\pi R$; reference=$2\pi R_0$
v	particle velocity
$\hat{V}$	RF peak voltage
x, x', y, y'	particle coordinates in Frenet-Serret coordinate system
$\beta = v/c$; β_0; β_s	normalized particle velocity; reference; synchronous
Δp	momentum offset
$\epsilon_{[\mathrm{u},]\mathrm{rms}}$	beam emittance (u = x, y, l, Y, Z, s, etc.)
ϵ_u	Courant-Snyder invariant (u = x, y, l, Y, Z, s, etc.)
ϕ_s	synchronous RF phase
$\gamma = E/m_0$	Lorentz factor
γ_u	optical function (u = x, y, Y, Z, l, etc.)
η	phase-slip factor
ρ	local curvature radius
θ	local azimuthal angle coordinate$^{(a)}$
ϑ	azimuthal coordinate$^{(b)}$
ζ	spiral angle of a spiral sector magnet field boundary

(a) In the polar coordinate system centered at the center of the FFAG ring.
(b) In the polar system with origin on a ϑ = *constant* spiral.

Introduction

The concept of fixed field alternating gradient (FFAG) accelerators dates back to the early 1950's [1, 2, 3]. At a time where fixed orbit strong focusing pulsed synchrotrons were taking over on the path to higher and higher energy, the FFAG method was explored as a way to implement the principles of strong focusing and synchrotron stability, with potential to yield high intensity rings, up to multi-GeV energy range in the case of proton beams.

Three electron prototypes were built and operated in the 1950's, by the Midwestern Universities Research Association [4]. Several proton rings have been built in Japan from the late 1990s on, exploiting latest technological progress regarding magnet design and acceleration systems [5].

FFAGs have often been proposed as an alternative to Linac, RCS or cyclotron, in various applications including proton drivers, protontherapy, fast acceleration of short-lived beams, etc.

0.1 Principles, basic maths

In the Frenet-Serret coordinate system moving along the reference orbit, transverse particle motion across the magnetic elements of a planar accelerator structure satisfies [6]

$$\begin{cases} x'' + \dfrac{(\gamma\beta)'}{(\gamma\beta)}x' + \dfrac{1-n}{\rho^2}x = 0 \\ y'' + \dfrac{(\gamma\beta)'}{(\gamma\beta)}y' + \dfrac{n}{\rho^2}y = 0 \end{cases} \tag{0.1}$$

wherein (*)'=d(*)/ds. These equations account for a possible slow change of momentum, via the damping term.

Considering for the moment fixed momentum, the damping term can be dropped ($(\beta\gamma)' = 0$). Introducing the azimuthal angle $\vartheta = s/R$, with $R = \mathcal{S}/2\pi$ and $\mathcal{S}$ the integrated path length over the closed orbit, Eq. 0.1 takes the form

$$\begin{cases} \dfrac{d^2x}{d\vartheta^2} + \left(\dfrac{R^2}{\rho^2(r,\vartheta)}\,[1-n]\right)x = 0 \\ \dfrac{d^2y}{d\vartheta^2} + \left(\dfrac{R^2}{\rho^2(r,\vartheta)}n\right)y = 0 \end{cases} \tag{0.2}$$

A sufficient condition for the betatron oscillations, and therefore the betatron tunes, to be independent of momentum is for the forcing terms to be such, which writes

$$\left.\frac{\partial n}{\partial p}\right|_{\vartheta=const} = 0 \tag{0.3}$$

$$\left.\frac{\partial}{\partial p}\left(\frac{R}{\rho}\right)\right|_{\vartheta=const} = 0 \tag{0.4}$$

The first equation tells that, at a given azimuth, the field index is independent of momentum, while the second one states the geometrical similarity of closed orbits which differ by their momentum, this is the scaling property of this type of FFAGs.

It results from these conditions that

$$k = \frac{R}{B}\frac{dB}{dR} \approx \frac{R}{B}\frac{dB}{dx} = -\frac{R}{\rho}n = const \tag{0.5}$$

and, by integration

$$B(R) = B_0\left(\frac{R}{R_0}\right)^k \tag{0.6}$$

Note in passing, given $k = constant$, it results that a reversed sign dipole ($\rho < 0$) introduces a reversed-sign field index n, which meets the key concept of strong ($|n| \gg 1$) alternating gradient focusing.

The rigidity, or momentum, dependent average orbit radius writes

$$\frac{R}{R_0} = \left(\frac{B\rho}{B\rho_0}\right)^{1/(k+1)} = \left(\frac{p}{p_0}\right)^{1/(k+1)} \tag{0.7}$$

In a general manner, in a lattice comprised of bends and field-free sections, the axial component of the magnetic field at location (r, θ) along an orbit in the median plane (y=0) satisfies

$$B(r, \vartheta) = B_0\left(\frac{r}{R_0}\right)^k \mathcal{F}(\vartheta) \tag{0.8}$$

where the $2\pi/N$-periodic flutter factor $\mathcal{F}(\vartheta)$ describes the azimuthal variation of the field (the "gaps and valleys" of the AVF cyclotron) in the (r, ϑ) system. In the case of a radial sector FFAG, ϑ coincides with θ and $\mathcal{F}(\vartheta) = constant$ determines a radius (see Sec. 0.1.1), whereas in a spiral sector FFAG $\mathcal{F}(\vartheta) = constant$ determines a spiral curve (see Sec. 0.1.2). A "flutter" can be computed and quantifies the departure of the fringe fall-off from a step (or "hard-edge") discontinuity, namely,

$$F = \frac{\overline{(B-\overline{B})^2}}{\overline{B}^2} \xrightarrow{hard-edge} \frac{R}{\rho} - 1 \tag{0.9}$$

with $\overline{(*)} = \int_{cell}(*)\,ds/\int_{cell} ds$ an average over the cell. R and the curvature radius ρ are related by the length of their common cord, namely

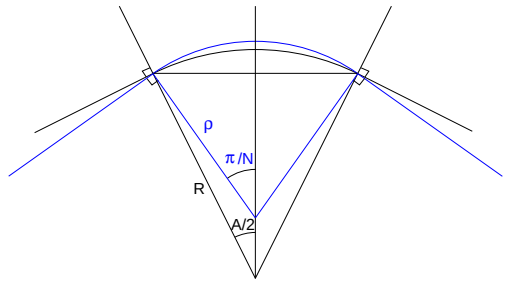

Fig. 0.1 Geometrical parameters in a sector dipole of a N-sector ring. The R-radius arc (black) is the line of constant, scaling field (Eq. 0.6). The ρ-radius arc (blue) represents a closed orbit, subject to a $2\pi/N$ deviation in the sector. Both arcs share the same cord (Eq. 0.10).

$$R\sin(A/2) = \rho\sin(\pi/N) \tag{0.10}$$

The packing factor takes the value

$$pf = \mathcal{L}/\mathcal{S} = A/(2\pi/N) \tag{0.11}$$

Orbits

In a general manner, closed orbits need be computed numerically, searching for the momentum-dependent closed periodic solution. They feature small amplitude scalloping in the vicinity of the circle with radius R(p) (Eq. 0.7), thus initial conditions for numerical search can be taken as $r \approx R(p)$ and r' very small.

The orbit length scales with momentum, following

$$\mathcal{S}(p) = \mathcal{S}_0 \left(\frac{p}{p_0}\right)^{\frac{1}{k+1}} \tag{0.12}$$

Focusing

There is two ways that the FFAG technique overcomes the limitations of weak focusing index ($0 < n < 1$),

- one consists in alternating strong transverse gradients (large $|n|$, see Eq. 0.5), which is achieved as pointed earlier by alternating normal-bend and reversed-bend magnets - however with the detrimental effect of decreased packing factor, increased circumference of the ring (more in Sec. 0.1.1),

- a second method is based on edge (or Thomas) focusing and uses spiral sector dipoles, where a large spiral angle (strong vertical focusing, horizontally defocusing) compensates the large field index (strong horizontal focusing, vertically defocusing) (more in Sec. 0.1.2).

It results from eq. 0.2 that particles experience similar betatron motion to that in fixed-orbit rings (betatron, pulsed synchrotron), with a subtlety though, however of marginal effect in general: from Eq. 0.1 it comes out that the transverse particle oscillations in the presence of varying momentum, due to acceleration, satisfy

$$x, y \propto \frac{\sqrt{R}}{\sqrt{\beta\gamma}} \tag{0.13}$$

$$x', y' \propto \frac{1}{\sqrt{R}\sqrt{\beta\gamma}} \tag{0.14}$$

thus the damping of betatron oscillations is R-dependent. Instead, the betatron damping of the transverse emittances of a beam is not,

$$\epsilon_{rms} = \left[< x^2 >< x'^2 > - < xx' >^2\right]^{1/2} \propto \frac{1}{\beta\gamma} \tag{0.15}$$

An approximation of the radial and axial tunes writes [6, Eq. 5.2]

$$\nu_r \approx \sqrt{1+k}, \quad \nu_y \approx \sqrt{-k + F^2(1 + 2\tan^2\zeta)} \tag{0.16}$$

not necessarily very accurate yet helpful in evaluating the respective effects of changes in k or F (or additionally ζ in the case of a spiral sector).

Longitudinal motion

The revolution time $T_{rev} = \mathcal{S}/\beta c$ can be written

$$T_{rev} = T_{rev,0}\left(\frac{p}{p_0}\right)^{\frac{1}{k+1}} \frac{\beta_0}{\beta} \tag{0.17}$$

with the index "0" referring to quantities which correspond to $R = R_0$. The momentum compaction and transition γ stem from p(R) (Eq. 0.7), namely

$$\alpha = \frac{\Delta R/R}{\Delta p/p} = \frac{1}{1+k} \quad \text{and} \quad \gamma_{tr} = \sqrt{1/\alpha} = \sqrt{1+k} \tag{0.18}$$

Acceleration in a scaling FFAG may use the synchro-cyclotron method. Longitudinal particle motion thus follows the principles of synchrotron phase stability, with the same theoretical approach. Momentum acceptance and synchrotron frequency thus write

$$\pm\frac{\Delta p}{p} = \pm\frac{1}{\beta_s}\left(\frac{2q\hat{V}}{\pi h\eta E_s}\right)^{1/2}, \quad \nu_s = \frac{2\pi}{\beta_s}\left(\frac{h\eta\cos\phi_s\, q\hat{V}}{2\pi E_s}\right)^{1/2} \tag{0.19}$$

On the other hand, fixed magnetic field allows flexibility on the RF programs. Diverse acceleration techniques have been explored or experimented, constituting as many interesting numerical simulation topics. These include

- multiple-bunch acceleration, by superposition of different frequency RF waves in the cavity [7],
- induction acceleration, which may be based on the use of a betatron core [8], or running the FFAG in betatron mode as part of a dual-technique acceleration cycle [9],
- in-bucket acceleration [10], a technique also envisioned for longitudinal phase rotation [11],
- high energy serpentine acceleration [12] in a quasi-isochronous scaling FFAG mode.

0.1.1 Radial Sector

A specimen of a proton radial sector scaling FFAG, a 150 MeV ring built and operated at KEK in the early 2000s, is shown in Fig. 0.2 [13]. The ring periodicity is N=12,

Fig. 0.2 KEK 150 MeV 12-cell scaling FFAG ring, and its cyclotron injector (left). Its lattice cell magnet: a DFD dipole triplet (right). The gap shape follows Eq. 0.20 so ensuring the scaling field law (Eq. 0.6).

a cell is comprised of a DFD dipole triplet and a drift. The gap shape in the three dipoles is of the form

$$g(R) = g_0 \left(\frac{R_0}{R}\right)^{\kappa} \qquad \text{with} \;\; \kappa \approx k \tag{0.20}$$

(greater (lower) gap at lower (greater) energy and radius) to ensure the scaling field law, Eq. 0.6. Table 0.1 summarizes the parameters of concern in these problems.

The accelerator is operated like a synchrotron-cyclotron. All concepts of synchro-cyclotron transverse motion and acceleration apply and can be referred to.

Table 0.1 Parameters of the KEK radial sector scaling FFAG.

Injection - extraction energy	MeV	12 - 150
Injection - extraction radius	m	4.7 - 5.2
Lattice		DFD
Number of cells (N)		12
Maximum β_r / β_z max.	m	3.8 / 1.3
Tunes, ν_r / ν_z		3.7 / 1.2
Magnet		
Type		DFD radial triplet
Sector angle (A), D / F	deg	3.43 / 10.24
Injection - extraction gap	cm	20 - 4
k		7.6
Min. - max. field, D / F	T	0.3-0.8 / 0.5-1.6
Acceleration		
Frequency swing	MHz	1.5 - 4.6
Harmonic		1
Voltage, peak-to-peak	kV	19
Cycle time	ms	4
Maximum repetition rate	Hz	250
Equivalent dB/dt	T/s	280
Synchrotron tune ν_s		0.039 - 0.012

0.1.2 Spiral Sector

A specimen spiral sector FFAG design is shown in Fig. 0.3. This is a protontherapy, variable energy (230 MeV maximum) and multiple extraction FFAG ring, aimed at cancer tumor treatment [14, 15].

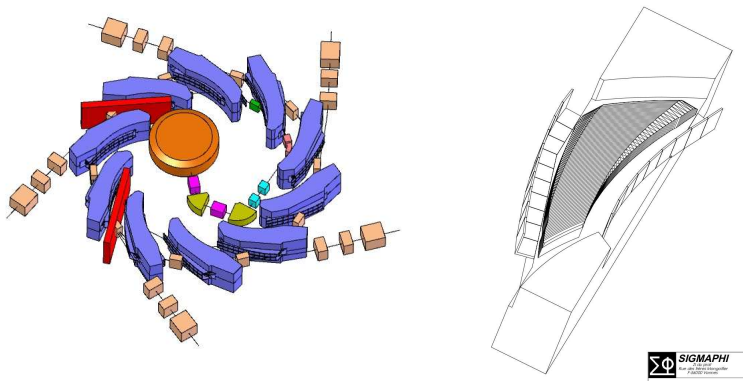

Fig. 0.3 RACCAM protontherapy scaling FFAG ring design, and its variable energy H- cyclotron injector (left). Engineer design of its spiral dipole half-yoke, showing the gap shaping pole, variable chamfers, and field clamps to ensure constant tunes (right).

The ring periodicity is N=10, a cell is comprised of a spiral sector dipole and a drift. The dipole magnet gap shape satisfies Eq. 0.20. Table 0.2 summarizes the parameters of the FFAG ring for skull and neck tumor treatment, 180 MeV operation. The RACCAM study included magnet prototyping and field measurements which covered up to 2 T operation, 230 MeV extraction energy [16, 17].

The median plane field at location (r, θ) in a spiral sector can be written under the form [18]

$$B(r) = B_0 \left(\frac{r}{r_0}\right)^k \mathcal{F}\left(\tan(\zeta) \ln \frac{r}{r_0} - N\theta\right) \tag{0.21}$$

The field boundaries of a spiral sector magnet are on a $\mathcal{F}(\vartheta) = constant$ curve, thus defined by

$$\vartheta = \theta - \tan\zeta \ln \frac{r}{r_0} = constant, \qquad i.e., \qquad r = r_0 \exp\left(\frac{\theta}{\tan\zeta}\right) \tag{0.22}$$

Closed orbits at different momenta are similar and differ by a double transform: homothety and rotation.

The RACCAM design operates a synchrotron-cyclotron, including single-bunch or multiturn injection, synchrotron acceleration, and single-turn extraction for bunch-

Table 0.2 Parameters of the RACCAM protontherapy spiral sector scaling FFAG ring. Some of the parameter values vary with variable operation energy: they are stated here over the extraction energy range 70 → 180 MeV.

		Injection		Extraction
energy, variable	MeV	5.55 → 15		70 → 180
$B\rho$	T.m	0.341 → 0.562		1.231 → 2.030
$B\rho_{extr.}/B\rho_{inj.}$ ratio			3.612	
$\beta\gamma$		0.109 → 0.180		0.393 → 0.648
Lattice type			spiral, scaling	
Number of cells (N)			10	
Packing factor (pf)			0.34	
Drift length	m	1.15		1.42
Orbit radius (R)	m	2.794		3.460
Orbit excursion (Eq. 0.7)	m		0.667	
Tunes ν_r; ν_y		constant: 2.76		1.55 → 1.60
Transition gamma (γ_{tr})			2.45	
Magnet				
Type			spiral sector	
Sector angle (A)	deg.		12.24	
Spiral angle (ζ)	deg.		53.7	
k			5.00	

to-pixel tumor irradiation [14]. All concepts of synchro-cyclotron transverse motion and acceleration apply and can be referred to.

0.2 Exercises

Checking the consistency of numerical results worked out in the exercises against theory (or vie-versa) is, even if not explicit, part of these exercises.

In the following exercises a superposition technique may be used to simulate the field in an N-tuple of neighboring magnets. The method consists in computing the mid-plane field at any location (r, θ) by adding individual contributions [19], namely,

$$B_y(r,\theta)\big|_{y=0} = \sum_{i=1,N} B_{y,i}(r,\theta)\big|_{y=0} = \sum_{i=1,N} B_{0,i}\,\mathcal{F}_i(r,\theta)\,\mathcal{R}_i(r) \tag{0.23}$$

with $\mathcal{R}_i(r) = (r/r_{0,i})^{k_i}$ (Eq. 0.6). Note that, in doing so it is not meant that field superposition does apply in reality (FFAG magnets are closely spaced, cross-talk may occurs), however it appears to allow closely reproducing magnet computation code outcomes.

0.2.1 KEK 150 MeV Radial Sector, DFD Triplet, FFAG

This series of exercises is based on the KEK 150 MeV radial sector FFAG shown in Fig. 0.2. The parameters of concern are given in Tab. 0.1.

0.1 Field in a Radial Sector Dipole Triplet Using the field modeling of Eq. 0.21, including soft field fall-offs, produce a 3D view of the median plane field of the sector triplet (*i.e.*, $(X, Y, B(X, Y))$ view, with X, Y taken in the magnet frame).

0.2 Orbits, Scalloping Finding the closed orbits is a necessary first stage prior to characterizing the focusing properties of the lattice. It also serves such purposes as computing the momentum dependence of optical functions (exercise 0.4), getting the time of flight law for acceleration (exercise 0.7), etc.
(a) Assume first a hard-edge magnet model, namely, referring the cell sketch in Fig. 0.2, non-zero field in the blue regions only, or equivalently, $\mathcal{F}(\theta) = \begin{cases} 1\ inside \\ 0\ outside \end{cases}$ *a dipole* in Eq. 0.6.
Compute a scan of the periodic orbits $y_p(\theta)$ across the cell, for a few proton energies ranging in $10 \leq E = p/\beta \leq 125$ MeV. Plot these $y_p(\theta)$, and in a separate graph the field along the orbits.
(b) Show graphically the homothety of the orbits in a laboratory coordinate system, on top of a footprint of the radial sector dipole triplet. Check the similarity ratio.
(c) Show that the orbit excursion from injection energy (radius R_{inj}) to extraction energy (radius R_{xtr}) writes

$$R_{xtr} - R_{inj} = r_0 \left(1 - \left(\frac{p_{inj}}{p_{xtr}}\right)^{\frac{1}{1+k}}\right) \tag{0.24}$$

Check this against closed orbits from simulations.
(d) Evaluate the orbit "scalloping", *i.e.*, the maximum value of $|r(\theta) - R|/R$. Plot the latter as a function of energy.
(e) Introduce fringe fields at all dipoles, assuming constant gap (assume $\mathcal{F}(\theta)$ describes the interval [0,1] over about a gap size), re-do (a), compare.

This latest model including fringe fields will be used from now on, this will allow stressing some paramount effects they may have regarding the scaling properties of the cell.

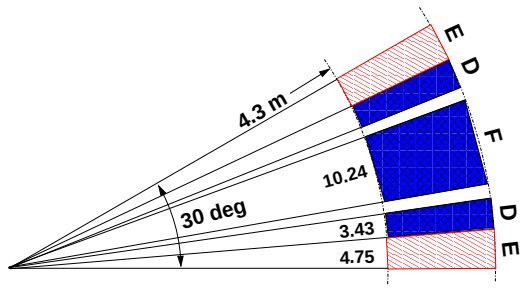

Fig. 0.4 Geometry of the 30 degree DFD cell. The shadowed 4.75 degree "E" regions represent the spacing between the dipole triplets around the ring.

0.3 Zero-Chromaticity (a) Compute and plot the momentum dependence of the radial and axial tunes, ν_r and ν_y. Use for that either one of two methods to obtain the tune values:
- from the cell transport matrix, or
- from the Fourier analysis of small amplitude motion through a few hundred cells.
Find the integer part of the tune in the case of the 12-cell ring (Fig. 0.2).
Compare with expectations (Eq. 0.16).
(b) It can be observed that the radial tune is constant with momentum, or equivalently with the orbit radius R, this is expected from the scaling law (Eq. 0.6). However the axial tune is r-dependent. Explain why.
(c) In the field model, introduce a r-dependence of the gap of the form Eq. 0.20. Note: this is equivalent to introducing a r-dependence of the fringe field extent, or equivalently of the field form factor $\mathcal{F}(\theta)$ in Eq. 0.8, proper to change the R-dependence of the axial focusing. Using an optimization ("fitting") procedure, compute the value of κ which minimizes the change of ν_y over the energy interval $10 < E < 125$ MeV.

0.4 Optical Functions Produce the betatron and dispersion functions through a cell, at 3, 15 and 30 MeV.
Check the value of the momentum compaction and transition γ_{tr}, their relationship to the horizontal tune.

0.5 Optical Tunability The B_F/B_D ratio of the F sector to D sector field, allows within some limits to change the betatron tunes. The axial one mostly. Produce samples of such ν_y adjustments, in a (ν_r, ν_y) graphic.

0.6 Stability Domain Assume different scaling index K_F and K_D in respectively the F and D sector. Produce a two-dimensional (ν_r, ν_y) tune scan diagram, covering the motion stability area resulting from varying K_F and K_D. Produce the corresponding (K_F, K_D) diagram.

0.7 Acceleration, Transverse Betatron Damping

0.2.2 A DF Doublet Spiral Sector FFAG

The ring considered here is based on a 24° degree cell, comprised of a pair of spiral sector FFAG dipoles with opposite signs (Fig. 0.5). The "wrong sign" bend contributes the overall size of the ring, however its purpose is to increase the flutter (the amplitude of the field step, Eq. 0.9), and thus the axial focusing (Eq. 0.16), which in turn allows greater radial focusing for a given spiral angle. As a matter of fact it is desirable for the latter not to exceed 55 $\sim$ 60 degree, for magnet and ring construction purposes.

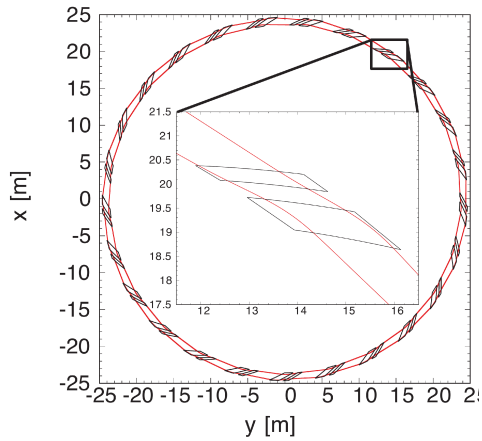

Fig. 0.5 A scheme of the 25-cell, spiral sector, FFAG ring. The cell, zoomed-in in the center, is based on an DF, spiral sector, FFAG dipole doublet. The two tracks are the injection and extraction closed orbits.

Table 0.3 Parameters of the RAL DF doublet radial sector scaling FFAG.

Kinetic energy	MeV	3 - 30
Reference radius (R_0)	m	4
Number of cells		15
Packing factor (*pf*)		0.35
Orbit excursion	m	0.6 m
Cell tune, H, V		0.212, 0.216
Ring tune, H, V		3.19, 3.24
Transition gamma		2.9
Magnet		
Type		spiral sector DF doublet
Sector angle (A), D / F	deg	2.4 / 4.8
Spiral angle (ζ)	deg	41
k		7.237
Field, D / F	T	-0.36 / 1
Ratio Bd/Bf		-0.36

0.8 Field in a Spiral Sector Dipole Doublet

Produce a 3D view of the median plane field of the spiral magnet (*i.e.*, $(X, Y, B(X, Y))$ view, with X, Y taken in the magnet frame). A possibility is to use the field modeling of Eq. 0.21,

0.9 Orbits, Scalloping Finding the closed orbits is a necessary first stage prior to characterizing the focusing properties of the lattice. It also serves such purposes as computing the momentum dependence of optical functions (exercise 0.11), getting the time of flight law for acceleration (exercise 0.13), etc.
(a) Compute a scan of the periodic orbits $y_p(\theta)$ across the cell, for a few proton energies ranging in $3 \leq E = p/\beta \leq 30\,\text{MeV}$. Plot these $y_p(\vartheta)$, and in a separate graph the field along the orbits.
Show the homothety-rotation of the orbits with a plot in a laboratory coordinate system, on top of a footprint of the spiral sector dipole.
(b) Illustrate graphically that the orbit "scalloping", *i.e.*, the maximum value of $|r(\vartheta) - R|/R$, is small $\forall E$, of the order of percents.
(c) This scan provides the momentum dependence of orbit length $\mathcal{S}(p)$ and thus average orbit radius $R(p) = \mathcal{S}/2\pi$. Give a graphical comparison to theory, Eq. 0.7.

0.10 Zero-Chromaticity Compute and plot the momentum dependence of the tunes, ν_r and ν_y. Use for that either one of two methods to obtain the tune values:
- from the cell transport matrix, or
- from the Fourier analysis of small amplitude motion through a few hundred cells.
Find the integer part of the ring tunes.

0.11 Optical Functions Produce the betatron and dispersion functions through a cell, at 3, 15 and 30 MeV.

0.12 Stability Domain Assume different scaling index K_F and K_D in respectively the F and D sector. Produce a two-dimensional (ν_r, ν_y) tune scan diagram, covering the motion stability area resulting from varying K_F and K_D. Produce the corresponding (K_F, K_D) diagram.

0.13 Acceleration, Betatron Damping Produce a simulation of a $3 \rightarrow 30\,\text{MeV}$ acceleration cycle in the 50-cell ring. Show that the (vertical, for simplicity) betatron oscillations satisfy the R-dependence of Eq. 0.13.
Accelerate a few 10s of particles and show the emittance damping of Eq. 0.15.

0.3 Solutions

0.3.1 KEK 150 MeV Radial Sector, DFD Triplet, FFAG

0.3.2 A DF Doublet Spiral Sector FFAG

0.8 Field in a Spiral Sector Dipole Doublet

A possibility is to generate a 3D plot directly from the analytical model (Eqs. 0.21 and 0.23). However, a field map may first be generated instead (and then plotted), this allows possibly further using it for ray-tracing (in a general manner, using a field map is a simple way to account for complicated fields, without the need of hard-coding them in the source tracking code).

Based on this goal, the spiral field model in zgoubi is deployed. A set of 81 trajectories, evenly spaced in r over the useful field radial extent, are tracked through the dipole. The angular integration step size is constant, $24^o/100$, and particle motion is forced to maintain constant radius r, throughout the dipole. This generates the mid-plane field over a $N_r \times N_\theta = 81 \times 100$ node 2D mesh.

Data file to generate and track 81 trajectories on constant radius, with constant integration angular step size:

```
CONSTY.dat
 'OBJET'
2.504760350042e+02   !  p=75090826.2, Etot=941272030.
1
81 1 1 1 1 1      ! This yields 81 radial mesh nodes.
1. 0. 0. 0. 0. 0.
380. 0. 0. 0. 0. 1.
'OPTIONS'
1 1
CONSTY ON

'MARKER'    S_Cell
'FFAG-SPI' ffag_spi
2                !   set to 2 for log to zgoubi.plt.
2 24. 400.   ! Numb. of dipoles; angle; reference R0.
-2.10000  0.  -3.49825720e+00 7.23737081e+00
3.951650121369e+00 -1.00000
4 1.4550e-01 2.26700  -6.3950e-01 1.15580  0.  0.  0.
1.20000  4.1000e+01 0.  0.  0.  0.
3.951650121369e+00 -1.00000
4 1.4550e-01 2.26700  -6.3950e-01 1.15580  0.  0.  0.
-1.20000  4.1000e+01 0.  0.  0.  0.
0.  -1.00000
0 0.  0.  0.  0.  0.  0.  0.
0.  0.  0.  0.  0.  0.
3.00000  0.  1.e+01 7.23737081e+00
3.951650121369e+00 -1.00000
4 1.4550e-01 2.26700  -6.3950e-01 1.15580  0.  0.  0.
2.40000  4.1000e+01 0.  0.  0.  0.
3.951650121369e+00 -1.00000
4 1.4550e-01 2.26700  -6.3950e-01 1.15580  0.  0.  0.
-2.40000  4.1000e+01 0.  0.  0.  0.
0.  -1.00000
0 0.  0.  0.  0.  0.  0.  0.
0.  0.  0.  0.  0.  0.
2 10             ! This step size (at R0) yields 101
1.67551608191    ! azimuthal mesh nodes.
2 0.  0.  0.  0.
'MARKER'    E_Cell
 'END'
```

Note: in the next exercises, the 'FFAG-SPI' section (on the left) is INCLUDed under the name 'spiralCell.inc[S_Cell:E_Cell]'

gnuplot instructions to plot from zgoubi.plt readout:

```
set title \
"Field map of spiral DF doublet, from zgoubi.plt."

set xlabel 'X [cm]'
set ylabel 'Y [cm]'
set zlabel 'B [kG]'

set hidden3d
set view 62, 292

splot "zgoubi.plt"  u  \
($10*cos($22)):($10*sin($22)<70? $10*sin($22):1/0):($25) \
with p pt 5 ps .8  lc palette  notit

pause 2
 set terminal postscript eps blacktext color
 set output "gnuplot_Zplt_fieldMap.eps"
 replot
exit
```

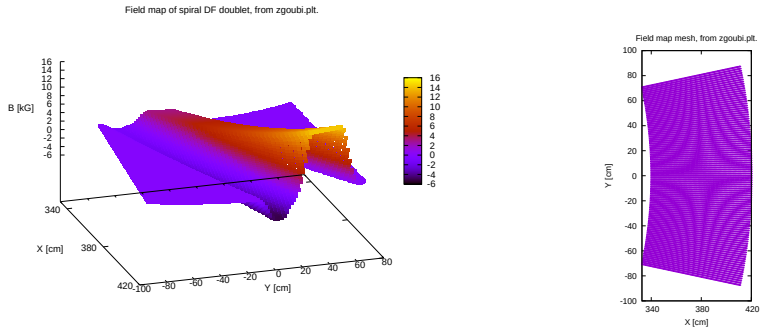

Fig. 0.6 Left: A field map of a spiral sector, generated by ray-tracing 101 trajectories evenly spaced in r, through the magnet as defined using an analytical model of the spiral sector geometry and field. Right: The $N_\vartheta \times N_r = 101 \times 81$ 2D mesh.

0.9 Orbits, Scalloping

(a) The zgoubi.dat file below (left) will first produce 31 closed orbits (FIT finds a closed orbit) for 31 different momenta (REBELOTE repeats) ranging in (relative) 1:3.18487667 (3-30 MeV). For each closed orbit its coordinates are stored in orbits.fai file (right after the FIT, prior to REBELOTE repeat). zgoubi.dat ends with a SYSTEM command which, once done with finding/storing the 31 periodic orbits, launches an additional, separate zgoubi.dat file (right). That file reads the former 31 periodic orbit coordinates from orbits.fai, it track them once through the magnet, and logs the trajectories in zgoubi.plt (due to IL=2 underneath 'FFAG-SPI') for further plot. The plot is launched by the next two gnuplot commands under that very SYSTEM, outcome in displayed in Fig. 0.7.

Spiral cell in data file:

```
ffag spiral
 'OBJET'
2.504760350042e+02     !  p=75090826.2, Etot=941272030
2
1 1
3.47689e+02 3.52251e+01 0. 0. 0. 1.000005373066e+00 'o'
1 1 1 1 1 1 1 1 1 1

'INCLUDE'
1
spiralCell.inc[S_Cell:E_Cell]

 'END'
```

To track the 31 orbits:

```
ffag spiral.   plotOrbits.dat file.
 'OBJET'     ! p=750908
2.50476035004e+02     ! gamma=1.003197366973
3
1 999 1
1 999 1
1. 1. 1. 1. 1. 1. 1. '*'
0. 0. 0. 0. 0. 0. 0.
0
orbits.fai

'INCLUDE'
1
spiralCell.inc[S_Cell:E_Cell]

'FAISCEAU'
 'END'
```

To scan over 31 different momenta and find the corresponding closed orbits: 'spiralCell.inc' under INCLUDE is the name of the data file on the left.

```
 ffag spiral
 'OBJET'       ! p=75090826.2, Etot=941272030,
2.50476035004e+02      ! gamma=1.003197366973.
2
1 1
3.476890234e+02 0.3522511766 0. 0. 0.  1. 'o'
1 1 1 1 1 1 1 1 1 1

 'FAISTORE'
orbits.fai storeOrbit ! Coordinates stored *after* FIT
1                     ! are closed orbit coordinates.

'INCLUDE'
1
spiralCell.inc[S_Cell:E_Cell]

'FIT2'
2  noFinal
1 30 0  2.
1 31 0  5.
2 1e-9 99            ! A 1e-9 penalty controls accuracy of
3.1 1 2 #End 0. 1. 0 ! convergence to periodic coordinates.
3.1 1 3 #End 0. 1. 0 ! 3.1: the constraint for periodicity.
 'MARKER' storeOrbit
 'REBELOTE'
31 0 0  1
1
OBJET  35  1:3.184876671929
'SYSTEM'
3                          ! 3 commnads follow.
./zgoubi -in plotOrbits.dat ! Launch a separate zgoubi.dat
gnuplot <./gnuplot_Zplt_XY.gnu  ! to track orbits.
gnuplot <./gnuplot_Zplt_XB.gnu
'END'
```

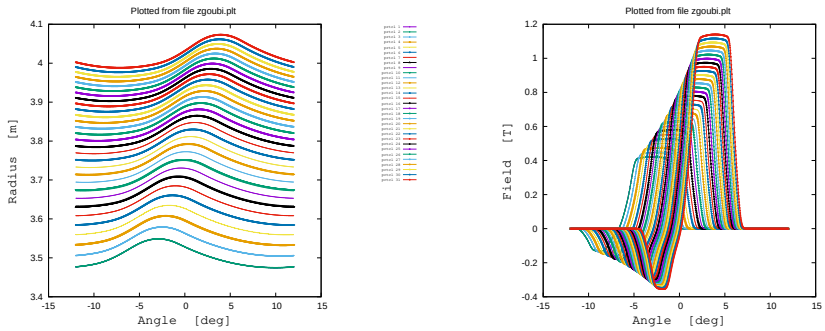

Fig. 0.7 Left: A plot of 31 energy dependent orbits across the 24° deg cell, $y_p(\vartheta)$, for proton energy ranging in 3-30 MeV. Right: Field experienced along these orbits.

0.10 Zero-Chromaticity

The file below will produce 31 sets of 11 sample particles spread around their respective closed orbits, for 11 different momenta ranging in (relative) 1:3.18487667 (3-30 MeV). From each 11-set a matrix is computed, tunes are derived using $\cos(\mu)$ =½Trace, these data are logged to zgoubi.MATRIX.out. A SYSTEM command launches a plot of the radial and axial tunes as read from the latter.

```
ffag spiral
 'OBJET'       ! p=75090826.2, Etot=941272030,
2.504760350042e+02   ! gamma=1.00319736
5
.001 .01 .001 .01 .001 .0001
3.47689023e+02 3.52251176e+01 0.  0.  0. 1. 'o'

 'FAISTORE'
orbits.fai    storeOrbit
1

'INCLUDE'
1
spiralCell.inc[S_Cell:E_Cell]

 'FIT2'
2  noFinal
1 30 0  2.
1 31 0  5.
2  1e-9 99  ! A 1e-9 penalty controls accuracy of
3.1 1 2 #End 0. 1. 0              ! convergence to
3.1 1 3 #End 0. 1. 0      ! periodic coordinates.

 'MATRIX' storeOrbit
1  11   PRINT

 'REBELOTE'
31 0 0  1
1
OBJET  35  1:3.184876671929
 'SYSTEM'
1
gnuplot < ./gnuplot_Qxy.vs.R.gnu
 'END'
```

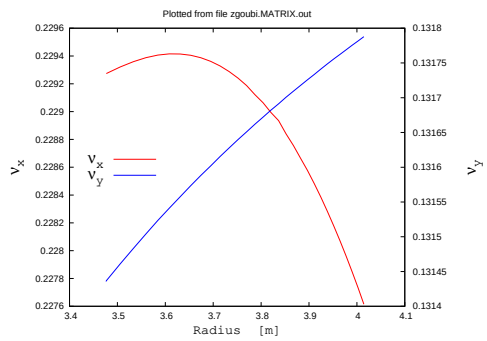

R-dependence of the tunes is weak ($\approx 10^{-3}$ radial, $3\,10^{-4}$ axial): the lattice is essentially zero-chromatic to first order in $\delta p/p$.

The ring tune is $360^o/24^o$ ×cell-tune = 15×cell-tune, that yields the integer part of the ring tune. More on that: write the betatron function over a cell under the form

$$\beta(s) = \overline{\beta} + \delta\beta(s) \quad \text{with} \quad \overline{\beta} = \int_{cell} \beta(s)ds \,/\, L$$

wherein β stands for β_r or β_y, $\int_{cell} \delta\beta(s)ds = 0$ and $L = \mathcal{S}/50$. Assume small enough betatron function modulation (see exercise **??**), so that $1/\beta(s) \approx (1 - \delta\beta(s)/\overline{\beta})/\overline{\beta}$. That yields

$$\overline{\left(\frac{1}{\beta}\right)} \approx \frac{1}{\overline{\beta}} - \frac{1}{\overline{\beta}^2\, L}\int_{cell} \delta\beta(s)ds = \frac{1}{\overline{\beta}}$$

so that cell tunes satisfy

$$\nu_{r,y} = \frac{1}{2\pi}\int_{cell} \frac{ds}{\beta_{r,y}(s)} = \frac{L}{2\pi}\overline{\left(\frac{1}{\beta_{r,y}}\right)} = \frac{L}{2\pi\overline{\beta_{r,y}}}$$

On the other hand, numerical results (or grossly, the square root of the mean value of the envelopes) yield $L/\overline{\beta_r} \approx 2.5$ and $L/\overline{\beta_y} \approx 1/2$, so that both cell tunes have zero integer part, and full tunes are just 50 times the fractional cell-tune values.

0.11 Optical Functions

The technique is the following:

(i) set IL=2 under 'FFAG-SPI'

(ii) track using OBJET/KOBJ=5 (it generates an 11-particle sample proper to matrix computation).

Due to (i), trajectories are stored step-by-step in zgoubi.plt. An off-line treatment program then computes the transport matrix from the 11 rays, step-by-step across the cell, which matrix is used in turn for stepwise transport of the beam matrix (a prior MATRIX, for instance the MATRIX scan of exercise 0.10, will provide the initial value of the periodic beam matrix). That program may be written in any convenient form - python, c, or else. Zgoubi toolbox provides a Fortran tool betaFromPlt which does that, together with gnuplot_betaFromPlt.gnu which does the plot. Repeat for all 3 energies, 10, 15 and 30 MeV.

The example of 30 MeV optical functions: zgoubi.dat files that tracks the 11-particle sample. It finishes with a SYSTEM call to the program which will transport the optical functions using the 11 tracks, and a SYSTEM call to a gnuplot file (below).

Note: in the solution to exercise 0.10 it was assumed that $1/\beta(s) \approx (1 - \delta\beta(s)/\overline{\beta})/\overline{\beta}$, based on small modulation of the betatron functions: does this hold?

```
ffag spiral
 'OBJET'
2.504760350042e+02     ! p=75090826.2, Etot=941272030.
5.1                    ! Will transport the beta functions.
.001 .01 .001 .01 .001 .0001
401.45997 -87.021578 0. 0. 0.   3.18488 'o'  ! Closed orbit.
0.7416 1.5008 -0.2278 0.8746 0. 1. 0.521 -0.104 0. 0. ! betas

'INCLUDE'
1
spiralCell.inc[S_Cell:E_Cell]

 'SYSTEM'
2
./betaFromPlt
gnuplot <./gnuplot_betaFromPlt.gnu
 'END'
```

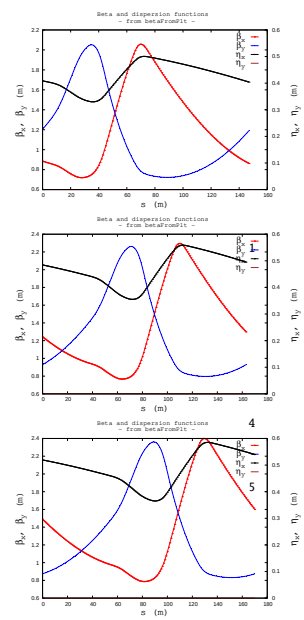

Optical functions through the cell at (from top to bottom) 3, 15 and 30 MeV.

An excerpt of gnuplot_betaFromPlt.gnu :

```
plot  \
     "betaFromPlt.out" u ($13):($2)  axes x1y1 w lp ps .1 pt 4 lw 2 lc rgb "red"  tit "{/Symbol b}_x"  ,\
     "betaFromPlt.out" u ($13):($4)  axes x1y1 w lp ps .1 pt 5 lw 2 lc rgb "blue" tit "{/Symbol b}_y"  ,\
     "betaFromPlt.out" u ($13):($7)  axes x1y2 w lp ps .1 pt 6 lw 2 lc rgb "black"  tit "{/Symbol h}_x"  ,\
     "betaFromPlt.out" u ($13):($9)  axes x1y2 w lp ps .1 pt 7 lw 2 lc rgb "brown" tit "{/Symbol h}_y"
```

0.12 Stability Domain

0.13 Acceleration, Betatron Damping

References

1. Kolomensky A. A., et al.: Some questions of the theory of cyclic accelerators. Ed. AN SSR, 1955, p. 7, PTE, No 2, 26 (1956).
2. Symon, K. R. Phys. Rev 100, 1247 (1955).
3. Concept presented by T. Ohkawa at a meeting of the Physical Society of Japan in 1953. After Albert L. Septier: Focusing of Charged Particles, Volume 2, Page 390 (1967).
4. F. Cole, O Camelot
5. FFAG R/D in Japan, 1999 on, review
6. Malek Haj Tahar, PhD Thesis, bnl tech note 2017
7. Mori, Y., et al.: Multi-beam acceleration in FFAG synchrotron. Proc. PAC 2001 Accel. Conf. 588-590 (2001).
   http://accelconf.web.cern.ch/AccelConf/p01/PAPERS/ROPA010.PDF
8. Tanigaki, M., et al.,: Construction of FFAG accelerators in KURRI for ADS study. Proc. EPAC 2004 Accel. Conf. 2676-2678 (2004).
   http://accelconf.web.cern.ch/accelconf/e04/PAPERS/THPLT078.PDF.
9. FFAG workshop: Combined betatron-synchrotron acceleration techinques in an ffag.
10. In-bucket muon acceleration at Japan NuFact
11. Sato, A., et al.: FFAG AS PHASE ROTATOR FOR THE PRISM PROJECTA. Proc. EPAC 2004 Accel. Conf. 713-715 (2004).
    http://accelconf.web.cern.ch/AccelConf/e04/PAPERS/MOPLT070.PDF
12. Yamakawa, E., et al.: Serpentine acceleration in zero-chromatic FFAG accelerators. Nuclear Instruments and Methods in Physics Research Section A: Accelerators, Spectrometers, Detectors and Associated Equipment, Volume 716, 11 July 2013, Pages 46-53.
13. KEK 150 MeV FFAG docu.
14. Antoine, S., et al.: Principle design of a protontherapy, rapid-cycling, variable energy spiral FFAG. NIM A 602 (2009) 293-305.
15. Fourrier, J., Martinache, F., Méot, F., Pasternak, J.: Spiral FFAG lattice design tools,application to 6-D tracking in a proton-therapy class lattice. NIM A 589 (2008) 133-142.
16. T. Planche et al., Design of a prototype gap shaping spiral dipole for a variable energy protontherapy FFAG,
    NIMA 604 (2009) 435-442.
17. IPAC10: field measurments at 2T, corresponding to 230MeV operation
18. F. T. Cole, MARK V expanded equations of motion, MURA/FTC-3, 19 Jan. 1956.
19. Méot, F., Lemuet, F.: Developments in the ray-tracing code Zgoubi for 6-D multiturn tracking in FFAG rings. NIM A 547 (2005) 638-651.
20. Kolomensky A. A. and Lebedev A. N.: Theory of Cyclic Accelerators. Northe Hollnad Publishing Company, Amterdam (1966). Original edition: Moscow, 1962.